Cell Reports Physical Science, Volume *5*

Supplemental information

Combined computational-experimental study of Ru(0)-catalyzed Guerbet reaction

Francesco Calcagno, Cristiana Cesari, Anna Gagliardi, Alessandro Messori, Andrea Piazzi, Filippo Tamassia, Marco Garavelli, Fahmi Himo, Rita Mazzoni, and Ivan Rivalta

Table of contents

S1. Supplementary Experimental Procedures

S1.1. Materials and methods

Diethyl ether (Et_2O) and tetrahydrofuran (THF) were distilled before use and stored in Schlenk flasks containing pre-dried molecular sieves. Ethanol (EtOH), toluene-d_8 and other solvents not previously listed were used without additional purification. The pre-catalyst species **1** was prepared as previously reported in ref [1]. All other reagents were purchased from commercial sources and were used as received, unless otherwise stated. Sodium ethoxide purity is 96%. Carbon isotopic labelling was done by adding a slight overpressure of ^{13}CO (≥ 99% atom ^{13}C) to the reactor.

NMR spectra were acquired at 298 K with a Varian Mercury Plus VX 400 (^1H, 399.9; ^{13}C, 100.6 MHz), or a Varian Inova 600 (^1H, 599.7; ^{13}C, 150.8 MHz) spectrometers. Chemical shifts were internally referenced to residual solvent peaks.

S1.2 General procedure for upgrading of ethanol

In a typical catalytic run, an oven-dried 6 mL Schlenk bomb fitted with a Teflon plug valve was charged with the ruthenium catalyst species **1** and the base, sodium ethoxide (NaOEt). Ethanol (0.5 mL, 8.6 mmol) was added, under inert atmosphere, to the reaction mixture. The reactor was sealed under inert atmosphere and heated at 150 °C, unless otherwise stated, under stirring for the desired reaction time. The microreactor was then cooled with an ice-water bath and subsequently opened. The reaction mixture was diluted by 3 mL of Et_2O and 162 µL of THF was added as internal standard. The resulting solution was analysed by Agilent Technologies 7890A GC system using a HP-5 capillary column Agilent 190915-413 (30 m x 0.35 mm, thickness 0.25 µm) in order to determine the ethanol conversion and product yields. Helium was used as carrier gas with a column flow of 0.909mL/min; the injector was maintained at a temperature of 230 °C in the split mode (40:1); total flow was 40.25 mL/min. The volume of solution injected was 0.5 µL and the method used was: starting oven temperature is 30°C (hold for 11 min) then heated to 270 at 30°C/min (hold for 5 min). Calibrations of all alcohols were performed by adding the same amount of THF (internal standard) to the different solutions and plotting the ratio A_a/A_s vs mol_a keeping constant the moles of standard. This procedure allows to avoid the measure of the total reaction volume obtaining the total amount of moles of analyte.

Compounds were also identified by GC-MS; in particular, we used an Agilent Technologies 6890 GC coupled with a mass spectrometer Agilent Technologies 5973 equipped with a non-polar column (5% Phenyl - 95% methylsiloxane), 30m x 250 µm x 1.05 µm. Helium was used as carrier gas at a flow rate in the column equal to 1ml/min; the injector was maintained at a temperature of 250 °C in the split mode (50:1); total flow was 23.9 mL/min. The volume of solution injected was 0.5 µL and the standard temperature program was the following: isothermal step at 40 °C for seven minutes, then the ramp of 10 °C/min until reach 250 °C, final isothermal step for 5 minutes. Light compounds were analyzed by sampling the reactor gaseous stream (once cooled at room temperature) by means of both GC-MS and a GC equipped with a TCD. The GC-MS was the same as for the liquid phase but the method was changed as follow: the volume injected was 0.5 mL and the standard temperature program start at 40 °C (maintained for ten minutes), then the ramp of 10 °C/min until reach 220 °C, final isothermal step for 2 minutes. Molecular hydrogen was detected by means of GC analysis using an Agilent Technologies 7890A Gas Chromatograph equipped with a TCD detector and Agilent 19095P-MS0S and a HP-molesieve capillary column (30 m x 0.530 mm, thickness 50 µm) with N_2 as carrier gas (column flow 3.0 mL/min). Headspace was sampled (0.04 mL) and manually injected into the instrument. The injector was maintained in split mode (5:1) at 150 °C. Oven

temperature was kept constant at 50 °C for the whole time of the analyses (5 minutes). The injection of pure reference standards allowed the comparison of retention times in the GC and GC-MS columns. The presence of carbon monoxide was detected with the same instruments as above, but equipped with an Agilent 7514 (27.5 m x 0.530 mm, thickness 25 μm) capillary column with H_2 as carrier gas (column flow 6.0 mL/min). The injector was maintained at 150 °C, whilst the oven temperature was kept constant at 50 °C for the whole time.

S1.3 Analysis of solids at the end of reaction

After a catalytical run (reaction conditions: **1**: 0.2 mol%; NaOEt: 20 mol%; T:150°C; t: 4 h) the mixture was diluted in 5 mL of diethyl ether. Upon filtration the solid residue was washed with diethyl ether until the solution becomes colourless. The solid collected was redissolved in water and dried on vacuum line (0.145 g), then dissolved in D_2O and analysed by ^{1}H-NMR spectroscopy.

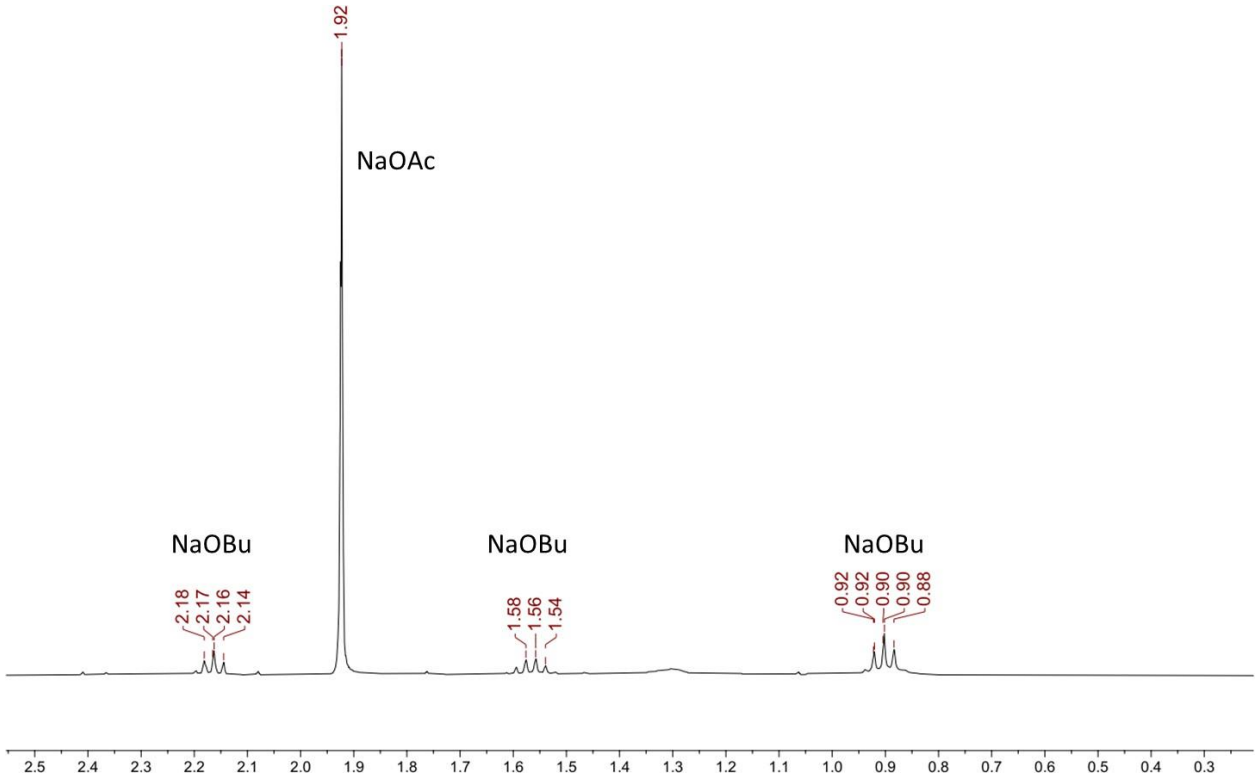

Figure S1. *^{1}H-NMR in D_2O of the solid obtained at the end of the reaction under best conditions (entry 4,* ***Table 1****) NaOAc = sodium acetate; NaOBu = sodium butanoate.*

S1.4 Recycle experiment

An oven-dried 6 mL Schlenk bomb fitted with a Teflon plug valve was loaded with the ruthenium catalyst **1** (0.0172 mmol) and NaOEt (1.72 mmol). Ethanol (0.5 mL, 8.6 mmol) was added under inert atmosphere and the reactor was sealed. The resulting reaction mixture was heated, under stirring, at 150 °C for 4 h. After cooling at room temperature, the alcohol mixture was removed under vacuum. Finally, new aliquots of EtOH (0.5 mL, 8.6 mmol) and NaOEt (1.72 mmol) were added under inert atmosphere to the solid residue and the following cycle was carried out as previously outlined.

S1.5 Procedure for upgrading of 1-butanol

An oven-dried 6 mL Schlenk bomb fitted with a Teflon plug valve was charged with the ruthenium catalyst **1** (0.2 mol%) and the base (20 or 10 mol%), sodium ethoxide (NaOEt). 1-Butanol (0.5 mL, 5.4 mmol) was added, under inert atmosphere, to the reaction mixture. The reactor was sealed under inert atmosphere and heated at 150 °C, for 4h. The microreactor was then cooled with an ice-water bath and subsequently opened. The reaction mixture was diluted by 3 mL of Et_2O and 162 µL of THF was added as internal standard. Characterization of the liquid and gas phase of the reaction crude has been performed as previously described for ethanol (paragraph 1.2).

S1.6 Larger scale experiments

Catalytic reactions were carried out in a 50 mL Schlenk bomb with a Teflon plug valve, in a 50 mL stainless steel autoclave or in a Teflon autoclave (300 mL) charged with the ruthenium pre-catalyst species **1** and NaOEt (20 mol%), then ethanol (5mL, 86mmol or 30 mL, 516mmol) was added. The reactor was sealed under inert atmosphere and, for the tests carried out under pressurized gasses, nitrogen or hydrogen was loaded in 10 or 20 bar. The resulting reaction mixture was heated, under stirring, at 150 °C for 4, 8 or 16 hours. After the reaction run time, the reactor was cooled to room temperature in an ice-water bath. The solution for GC analysis has been prepared diluting the sample in Et_2O and maintaining the same standard (THF) concentration.

S1.7 Procedure for ^{13}CO enrichment experiment

The reaction environment was set as described in the previous section with species **1** (0.0358 mmol), NaOEt (0.179 mmol) and EtOH (0.5 mL) under inert atmosphere (N_2). Molecular nitrogen was then replaced with a ^{13}CO-enriched pressurized atmosphere. The mixture was stirred at 150°C for 1 hour and cooled down in an ice-water bath. Next, it was dried with a high-vacuum pump and the resulting yellow power was dissolved in toluene-d_8 (0.5 mL) and filtered. The sample was analyzed using ^{13}C-NMR spectroscopy.

S2. The Cannizzaro and Tishchenko reactions in the Guerbet conditions

The Cannizzaro reaction converts two equivalents of aldehyde to one equivalent of carboxylic acid plus one of alkoxide (**Scheme S1**).[2] This reaction is promoted by sodium hydroxide NaOH, which is produced during the Guerbet reaction by the hydrolysis of sodium ethoxide NaOEt (pK_a(EtOH) = 15.90 at 25 °C).[3]

Similarly to the Cannizzaro reaction, the Tishchenko reaction converts two equivalents of aldehyde to one equivalent of ester in the presence of an alkoxide, e.g. NaOEt, instead of NaOH (**Scheme S1**).[2] Interestingly, in the presence of NaOH, the ester product of the Tishchenko reaction can be involved in the transesterification to a carboxylic acid and alkoxide. This saponification process leads to the same products of the Cannizzaro reaction (**Scheme S1**).

All these reactions occur during the Guerbet process and lead to a side consumption of ethanol, which lowers the overall yield to alcohols.[4]

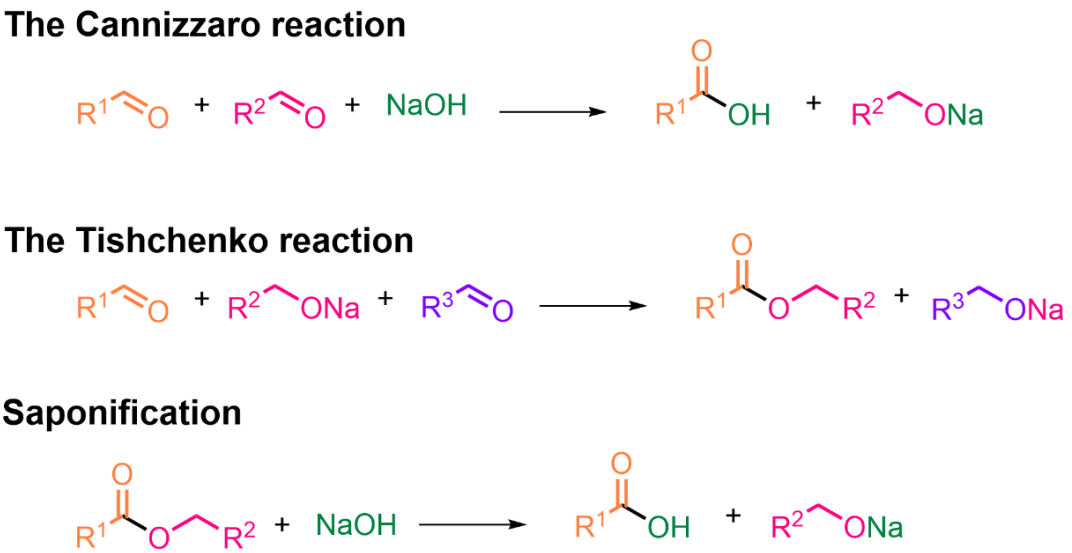

Scheme S1. *General reaction schemes for the Cannizzaro and the Tishchenko reactions and the saponification process.*

S3. Additional experiments

S3.1 Reaction behavior on waste ethanol

Table S1 shows that the use of different qualities of ethanol does not seriously affect the catalytic activity, demonstrating that the catalytic system composed by catalyst **1** and NaOEt is robust toward the presence of water and distillation by-products in the ethanol. **Table S1** reports tests done with ethanol purchased from Merck and two samples deriving from the head and tails of ethanol distillation provided by the CAVIRO S.p.A.

Table S1. *Effect of the quality of starting EtOH on the performance of the Guerbet reaction.*

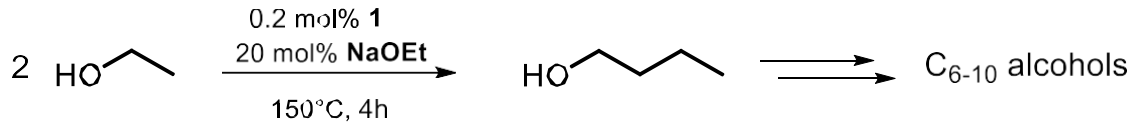

entry	**1** (mol%)	EtOH	Conversion EtOH (%)	Yield BuOH (%)	Yield (C_{4-10}) (%)	C-loss (%)	Selecivity (C_{4-10}) (%)
1	0.2	Merck[a]	53	36	47	6	89
2	0.2	CAVIRO AA[b]	54	32	44	10	81
3	0.2	CAVIRO 95%[c]	46	27	35	11	76
4	0.02	Merck[a]	58	30	50	8	86
5	0.02	CAVIRO AA[b]	49	27	46	3	94
6	0.02	CAVIRO 95%[c]	48	29	41	7	85

[a] *Code: 24105-1L-M.*
[b] *Absolute alcohol.*
[c] *For the composition, see batch analyses in Table S2.*

Table S2*. Composition of EtOH called CAVIRO 95%.*

Entry	Component	Amount (mg/100 mL AA)
1	Acetaldehyde	73.20
2	Methanol	127.93
3	Acetal	512.85
4	1-Propanol	383.52
5	1-Butanol	N.R.
6	Isobutanol	77.35
7	2-Butanol	4.55
8	Furfural	N.R.
9	Isoamyl alcohol	0.19
10	1-Hexanol	N.R.
11	2-Phenylethanol	N.R.
12	Ethyl acetate	98.85
13	Isoamyl acetate	0.25
14	2-Butanone	2.41
15	Paraldehyde	N.R.
16	Allyl alcohol	0.18
17	Benzyl alcohol	N.R.
18	Ethyl lactate	N.R.

S3.2 ^{13}C-NMR spectrum after ^{13}CO isotopic labelling experiment

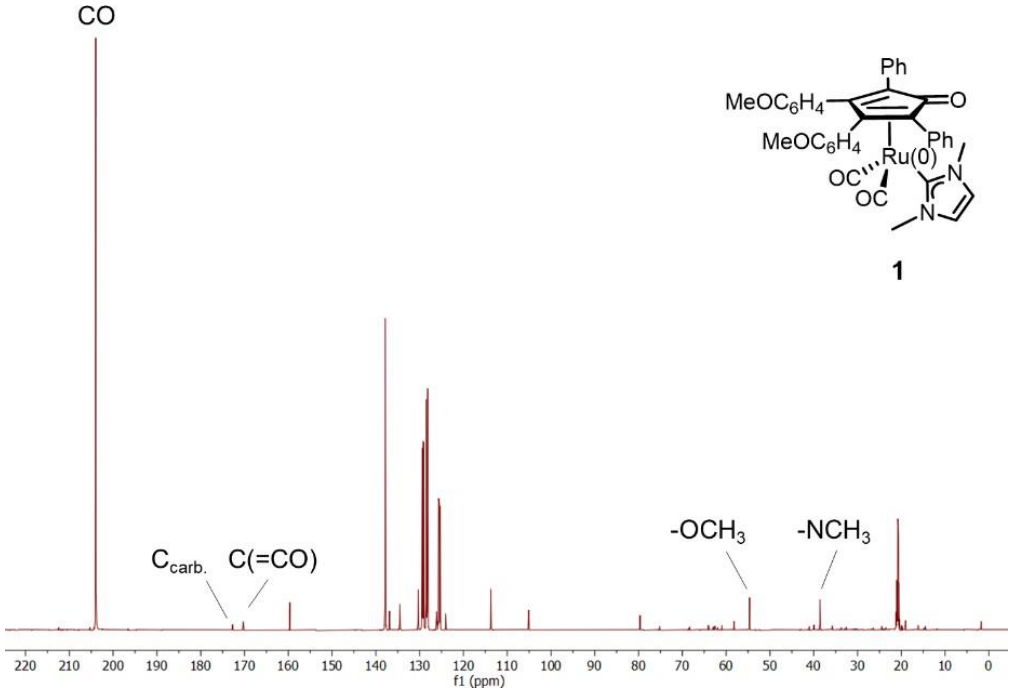

Figure S2. *Experimental ^{13}C-NMR spectrum recorded in toluene-d_8, showing a very intense peak at 204 ppm, respect to other characteristic signals of the catalyst* ***1****, confirming the isotopic labelling of a carbon monoxide ligand.*

S3.3. GC-MS spectrum of intermediate characterization test

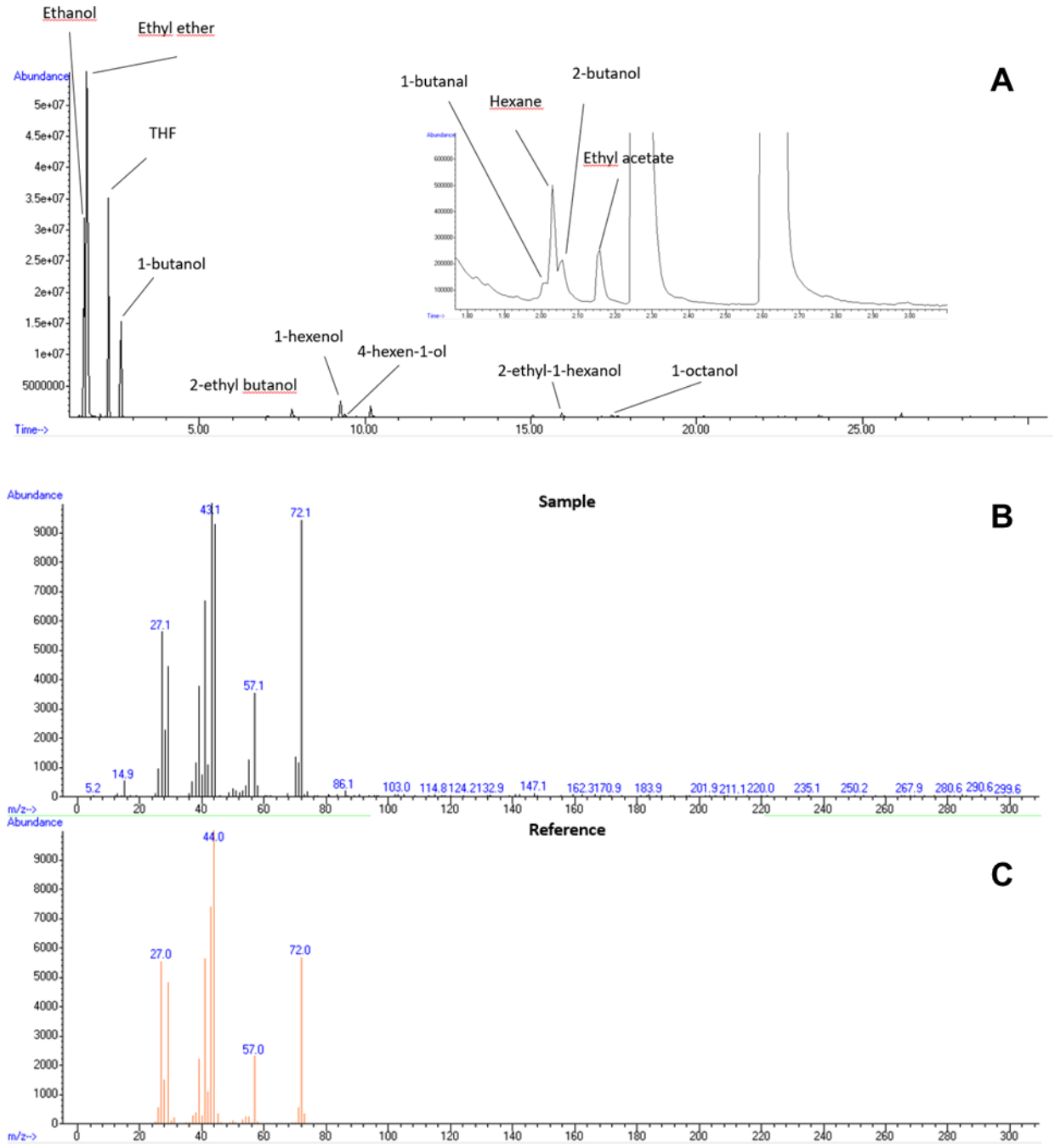

Figure S3. *(**A**) GC analysis with attribution of most important peaks. In the inset, a zoom of the time window related to 1-butanal. (**B**) Recorded MS spectrum of peak at 2.0 min in GC analysis is reported and compared to the reference MS spectrum of 1-butanal (**C**).*

S4. Computational details

All density functional theory (DFT) calculations were performed using the B3LYP exchange-correlation functional,[5–9] as implemented in the Gaussian16 software package.[10] Geometry optimizations were carried out in gas-phase using the 6-31G(d,p) basis set[11] for the H, C, N, O and Na elements, while the LANL2DZ basis set with pseudopotential[12] for was used for the Ru element. The nature of stationary points as minima (no imaginary frequencies) or transition states (one imaginary frequency) was characterized computing analytical frequencies at the same level of theory used for geometry optimizations. A manual conformational analysis was done for each stationary point in order to locate the conformer with the lowest energy. The influence of the inclusion of solvent and dispersion effects during the geometry optimizations was investigated by re-optimizing the geometries of stationary points along the main reaction steps with the B3LYP-D3 functional and in the presence of implicit solvent, using a polarizable continuum model (PCM)[13] for the ethanol.

The final energies reported in the present work were obtained by single-point calculations with larger basis set, i.e. 6-311+G(2d,2p),[14–17] the H, C, N, O and Na elements, and LANL2DZ basis set the Ru element. Corrections for dispersion effects using the Grimme-D3 dispersion scheme,[18] solvation effects using PCM, and thermal effects at 150 °C (the same used for the catalytic experiments) obtained from the frequency calculations were added.

The kinetic simulations were carried out using the LSODA algorithm[19] for ordinary differential equations (ODEs), as implemented in the COPASI software (version 4.30, build 240).[20]

S5. DFT insights

S5.1 Details of competitive activation mechanisms of catalyst 1

Figures S4 and **S5** show the energy profiles of the activation of catalyst **1** and the following dehydrogenation of the ethanol investigated in the present work.

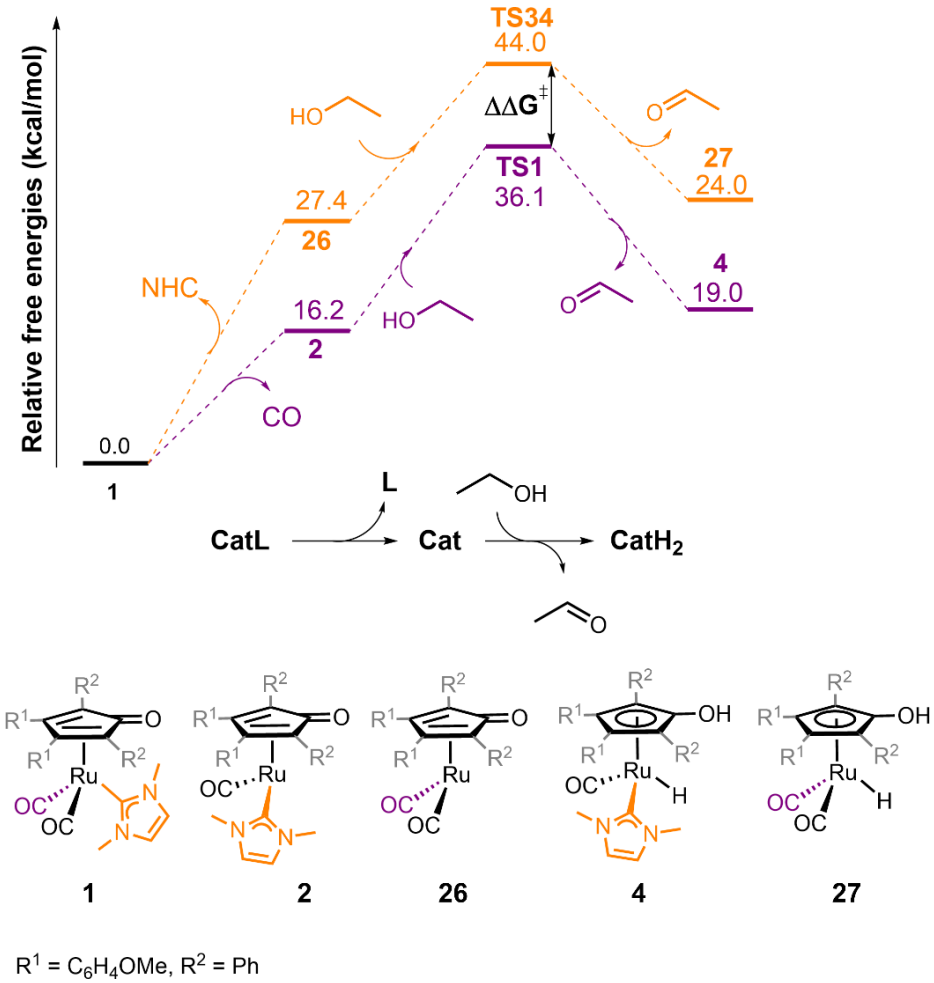

R^1 = C_6H_4OMe, R^2 = Ph

Figure S4*. Computed energy profiles (top panel) for two different activation pathways of the pre-catalyst* ***1****, i.e. via either CO (violet) or NHC (orange) dissociation, followed by the corresponding dehydrogenation of ethanol, at the B3LYP-D3/6-311+G(2d,2p)/LANL2DZ/PCM(ethanol)//B3LYP/6-31G(d,p)/LANL2DZ level of theory. The species involved in these reaction steps are shown in the bottom panel.*

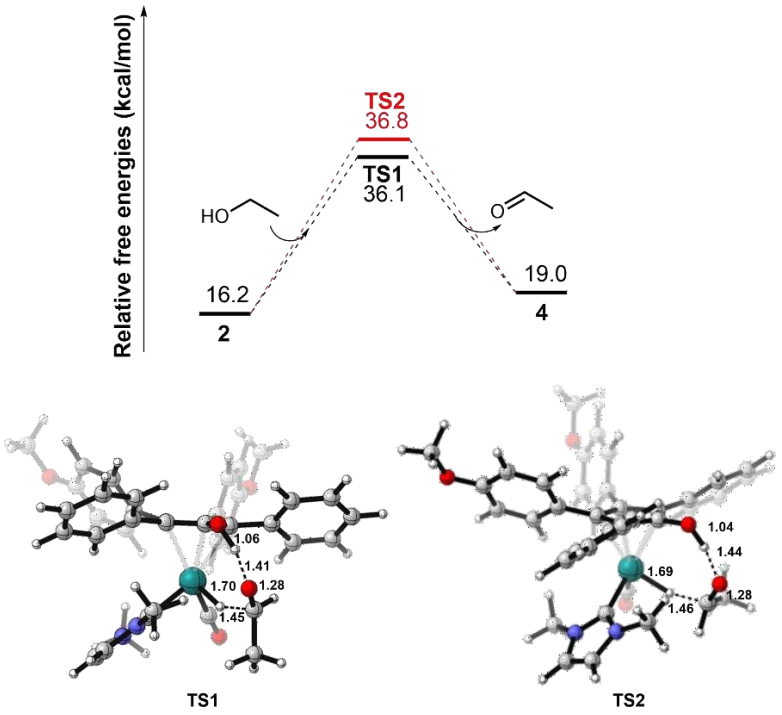

Figure S5*. Computed energy profiles (top panel) of dehydrogenation of ethanol through two competing diastereomeric transition states (**TS1** and **TS2**) at the B3LYP-D3/6-311+G(2d,2p)/LANL2DZ/PCM(ethanol)//B3LYP/6-31G(d,p)/LANL2DZ level of theory, and (bottom panel) the optimized geometries of the corresponding transition states.*

S5.2 Details on diastereomeric transition states involved in the hydrogenation process

Scheme S2 and **Figure S6** show possible reaction pathways for the double hydrogenation of (*E*/*Z*)-crotonaldehyde **11E**/**11Z** to 1-butanol **16**, comprising the diastereomeric transition states which are not discussed in the main text.

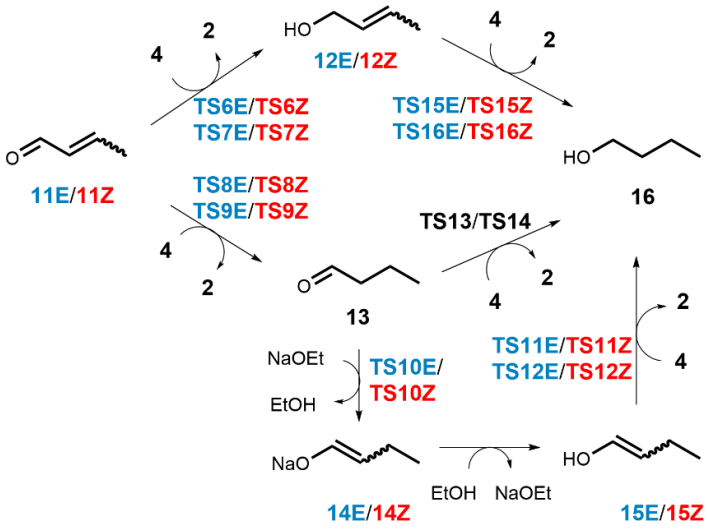

Scheme S2*. Competitive hydrogenation pathways suggested by DFT calculations, comprising the diastereomeric transition states.*

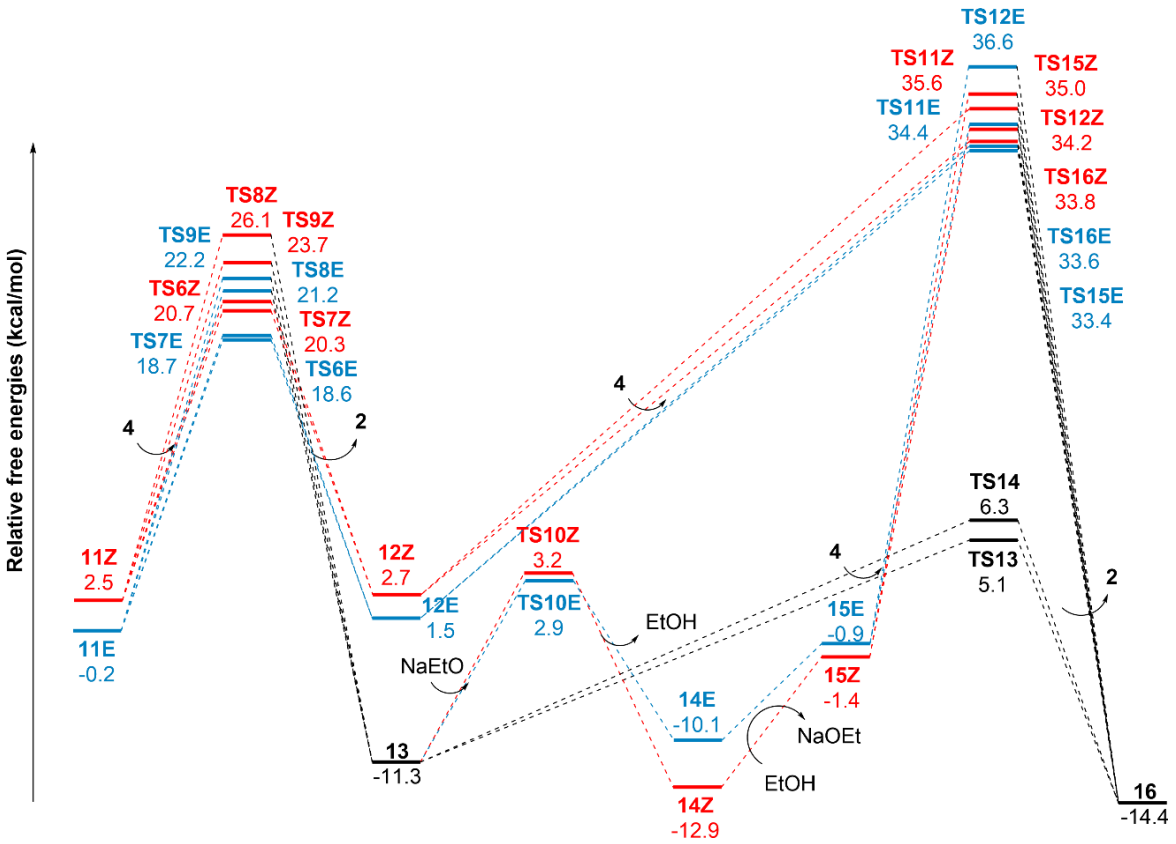

Figure S6*. Calculated free energy profiles for the double hydrogenation of (E/Z)-crotonaldehydes (**11E/11Z**) to 1-butanol (**16**), comprising the diastereomeric transition states, at the B3LYP-D3/6-311+G(2d,2p)/LANL2DZ/PCM(ethanol)//B3LYP/6-31G(d,p)/LANL2DZ level of theory.*

S5.3 Homologation to 1-hexanol

Homologation of 1-butanol (**16**) to 1-hexanol (**25**) follows a similar reaction mechanism as the one described for the homologation of ethanol to 1-butanol. The results are given in **Figures S7** and **S8** and **Scheme S3**, while the overall reaction mechanism is shown in **Scheme 4**.

One difference that should be mentioned, however, is that for the C-C coupling step between the acetaldehyde **5** and the 1-butanal **13**, the transition state corresponding to the coupling between the enolate **7** and the **13** could be obtained (**TS17**, **Figure S7**). In the case of the C-C coupling step between two equivalents of **5**, it was not possible to locate the transition state in the gas-phase, as discussed in the main text. However, the energy barrier corresponding to the **TS17** should be considered an approximated value, since it was possible to locate only one of the two asymmetric transition states which are possible for this step.

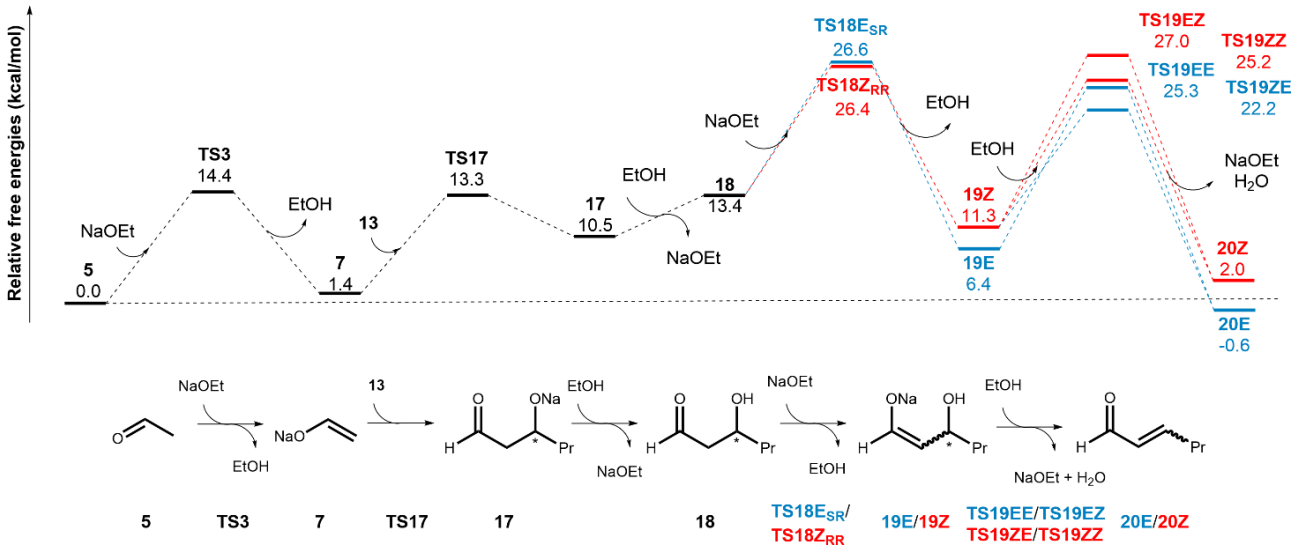

Figure S7. *Computed free energy profiles for the base-catalyzed aldol condensation between 1-butanal (**13**) and acetaldehyde (**5**) at the B3LYP-D3/6-311+G(2d,2p)/LANL2DZ/PCM(ethanol)//B3LYP/6-31G(d,p)/LANL2DZ level of theory. The species involved in the reaction steps are shown in the bottom panel.*

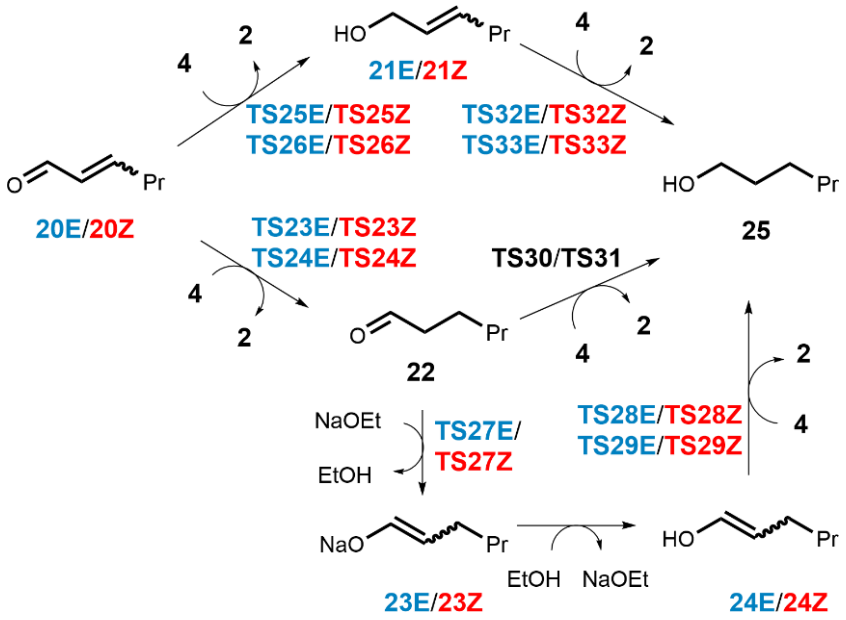

Scheme S3. *Competitive hydrogenation pathways suggested by DFT calculations, comprising the diastereomeric transition states, at the B3LYP-D3/6-311+G(2d,2p)/LANL2DZ/PCM(ethanol)//B3LYP/6-31G(d,p)/LANL2DZ level of theory.*

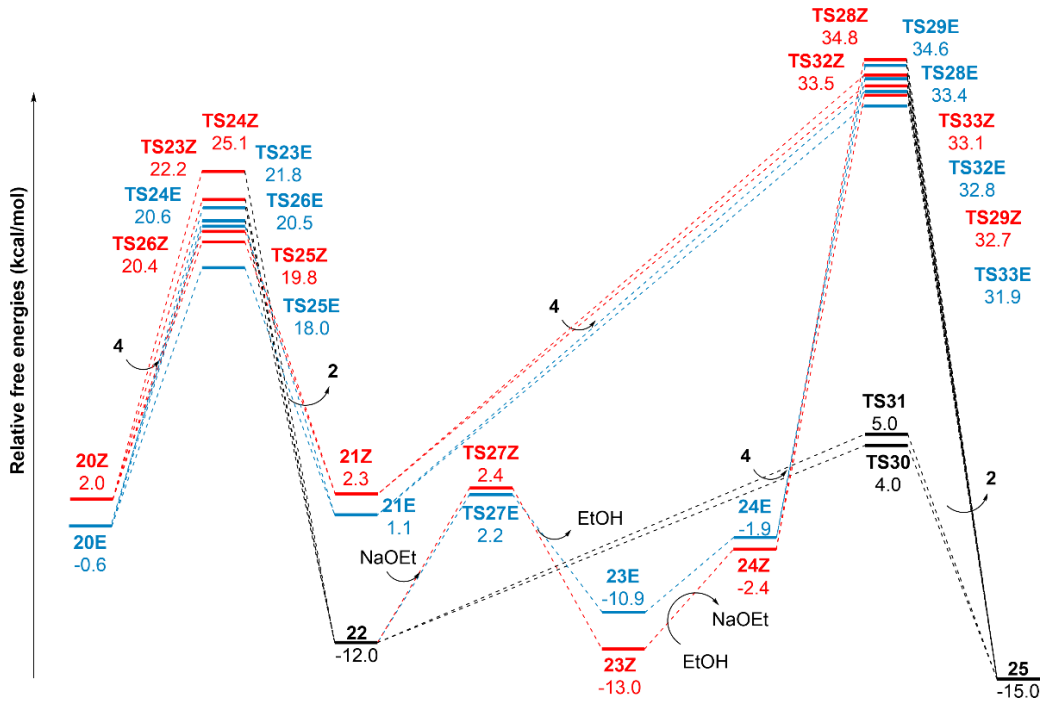

Figure S8. *Calculated free energy profiles for double hydrogenation of* ***20E/20Z*** *to* ***25****, comprising the diastereomeric transition states, at the B3LYP-D3/6-311+G(2d,2p)/LANL2DZ/PCM(ethanol)//B3LYP/6-31G(d,p)/LANL2DZ level of theory.*

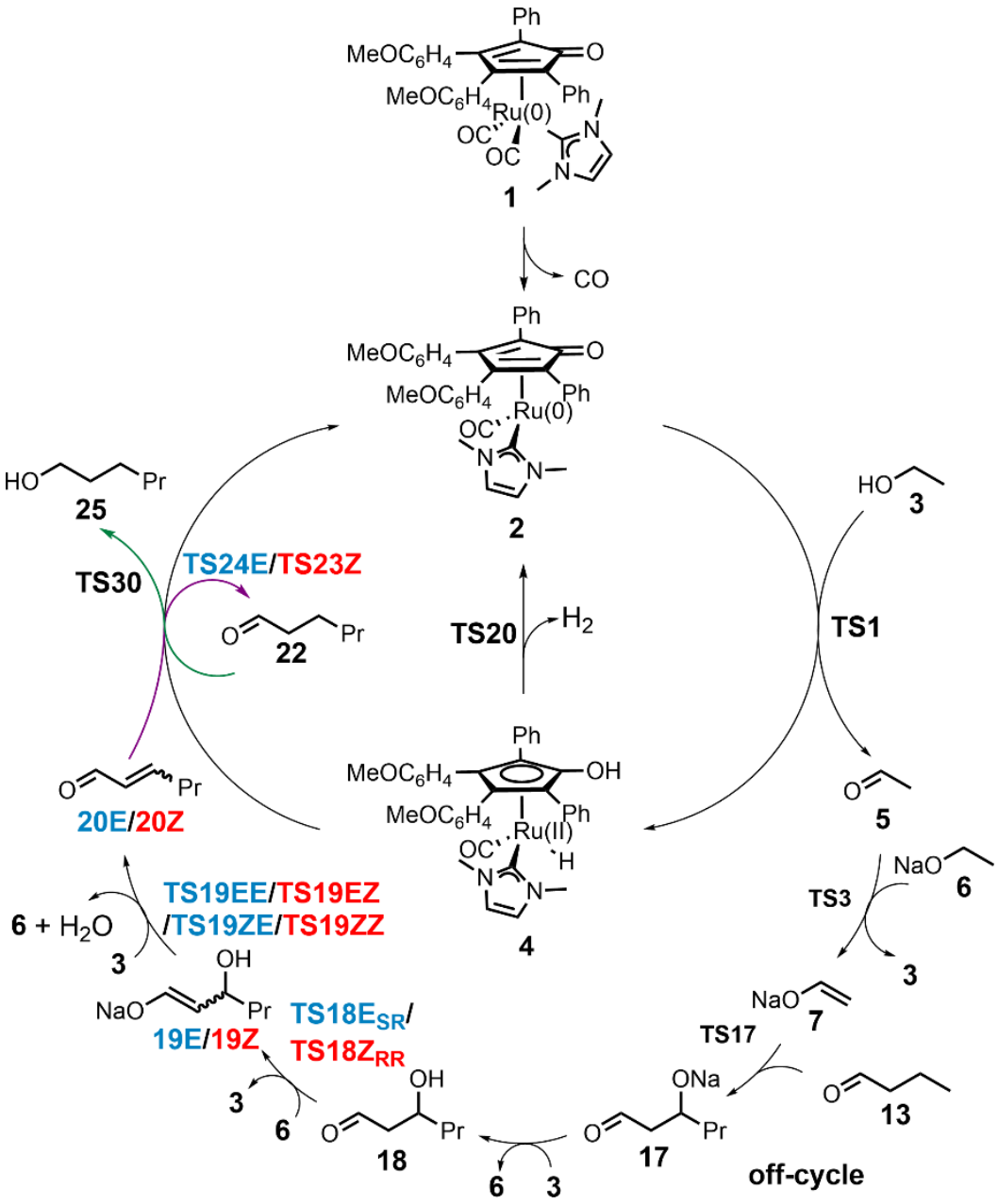

Scheme S4*. Guerbet reaction mechanism for the homologation of 1-butanol to 1-hexanol.*

S5.4 Including solvation and dispersion effects during geometry optimizations

In this section, the effect of using an optimization scheme that includes dispersions and implicit solvation effects on the energetics of the Guerbet reaction is presented. The MEPs presented in the main text for the homologation of ethanol to 1-butanol were computed using geometries optimized in the gas-phase, but the free energies of the stationary points were refined with single point computations using larger basis sets and including solvation and dispersion effects (see Computational details). Here, we compared these results with those obtained by including solvation and dispersion effects during geometry optimizations for the main reaction steps.

Table S3 shows the variations of the activation energies for the elementary steps considered. In the case of $TS^{c}_{7\_8}$, the variation is 6.2 kcal/mol (entry 4, **Table S3**), but it must be recalled that this transition state could not be characterized using the gas-phase and dispersion-free geometry optimizations, as mentioned in the main text. Thus, this variation refers to the difference between an activation barrier height and a barrierless endergonic process. Similar variations (3.6-6.2 kcal/mol) were found for the backward reactions of the elementary steps producing the 10E/10Z intermediates, as these species get stabilized once their geometries are optimized in solvent and with dispersions corrections. Next largest variations involve the activation barriers of the **TS5EE**, **TS5EZ**, **TS5ZE**, and **TS5ZZ** transition states, which vary around 3.3-3.7 kcal/mol (see **Table S3**).

Even if these variations in activation barriers are not negligible, it is important to highlight that they do not modify the picture of the reaction mechanism discussed in the main text. This is because the energetics of the rate-determining steps of the Guerbet reaction are not significantly altered by using geometries optimized including solvent and dispersions effects, as shown in **Figure S6**. Moreover, as reported in **Table S4**, the variations for the thermochemistry of the net reactions of the key steps of the Guerbet reaction, i.e. the dehydrogenation of ethanol to acetaldehyde, its aldol condensation to (*E/Z*)-crotonaldehyde, the hydrogenations of **11E**/**11Z** to 1-butanol, are minor (**Table S4**). In fact, the thermodynamics of the net processes vary < 0.3 kcal/mol (entry 3, **Table S4**), while the corresponding energy barriers vary < 2.3 kcal/mol (entry 4, **Table S4**).

Table S3*. The forward (**$\Delta G^{\ddagger}_{forward}$**) and backward (**$\Delta G^{\ddagger}_{backward}$**) free energy barriers of elementary steps calculated at the B3LYP-D3/6-311+G(2d,2p)/LANL2DZ/PCM(ethanol) level using either B3LYP/6-31G(d,p)/LANL2DZ or B3LYP-D3/6-31G(d,p)/LANL2DZ/PCM(ethanol) as geometry optimization method, are reported. The corresponding energy variations (**$\Delta\Delta G^{\ddagger}$**) are also reported. All energies are reported in kcal/mol.*

			B3LYP/ 6-31G(d,p)/ LANL2DZ		B3LYP-D3/ 6-31G(d,p)/LANL2DZ/ PCM(ethanol)			
entry	**Elementary step**	**TS**	**$\Delta G^{\ddagger}_{forward}$**	**$\Delta G^{\ddagger}_{backward}$**	**$\Delta G^{\ddagger}_{forward}$**	**$\Delta G^{\ddagger}_{backward}$**	**$\Delta\Delta G^{\ddagger}_{forward}$**	**$\Delta\Delta G^{\ddagger}_{backward}$**
1	**1 ⇋ 2 + CO**	N/A	16.2	0.0	16.2	0.0	-0.1	0.0
2	**2 + 3 ⇋ 4 + 5**	**TS1**	19.8	17.1	19.1	16.1	-0.8	-1.0
3	**5 + 6 ⇋ 3 + 7**	**TS3**	14.4	13.0	14.3	16.3	0.0	3.3
4	**5 + 7 = 8**	**TS_{7_8}**	8.8	0.0	15.0	3.8	6.2	3.8
5	**3 + 8 ⇋ 6 + 9**	N/A	3.0	0.0	3.9	0.0	0.8	0.0
6	**6 + 9 ⇋ 3 + 10E**	**$TS4E_{SR}$**	13.5	16.3	14.8	22.5	1.4	6.2
7	**6 + 9 ⇋ 3 + 10Z**	**$TS4Z_{RR}$**	13.5	14.4	13.6	17.9	0.0	3.6
8	**3 + 10E ⇋ 6 + H_2O + 11E**	**TS5EE**	14.4	25.0	17.9	23.6	3.6	-1.4
9	**3 + 10E ⇋ 6 + H_2O + 11Z**	**TS5EZ**	16.8	24.7	20.1	23.1	3.3	-1.7
10	**3 + 10Z ⇋ 6 + H_2O + 11E**	**TS5ZE**	9.6	22.3	13.4	22.4	3.7	0.1
11	**3 + 10Z ⇋ 6 + H_2O + 11Z**	**TS5ZZ**	12.6	22.5	16.1	22.4	3.5	-0.2
12	**4 + 11E ⇋ 2 + 13**	**TS8E**	21.5	32.5	22.4	33.5	1.0	1.0
13	**4 + 11Z ⇋ 2 + 13**	**TS9Z**	21.2	35.0	20.7	34.6	-0.5	-0.4
14	**4 + 13 ⇋ 2 + 16**	**TS13**	16.4	19.5	16.4	19.7	0.0	0.2
15[a]	**4 ⇋ 2 + $H_{2(sol)}$**	**TS20**	20.6	21.8	22.9	24.4	2.4	2.5

[a] *This step corresponds to entry 26 in the complete network reported in Table S5.*

***Table S4**. The free reaction energies (**ΔG**) and corresponding activation barriers (**ΔG‡**) for the dehydrogenation of ethanol (**3**) to acetaldehyde (**5**), the aldol condensation of **5** to (E/Z)-crotonaldehyde (**11E**/**11Z**) and their hydrogenation to 1-butanol (**16**), and the hydrogen loss steps, calculated at the B3LYP-D3/6-311+G(2d,2p)/LANL2DZ/PCM(ethanol) level using either B3LYP/6-31G(d,p)/LANL2DZ or B3LYP-D3/6-31G(d,p)/LANL2DZ/PCM(ethanol) as geometry optimization method, are reported. The corresponding energy variations (**ΔΔG** and **ΔΔG‡**) are also reported.*

		B3LYP/ 6-31G(d,p) LANL2DZ		**B3LYP-D3/ 6-31G(d,p)/LANL2DZ/ PCM(ethanol)**			
entry	**Net reaction**	**ΔG‡[a]**	**ΔG[a]**	**ΔG‡[a]**	**ΔG[a]**	**ΔΔG‡[a]**	**ΔΔG[a]**
1	**1 + 3 ⇋ CO + 4 + 5**	36.1	19.0	35.2	19.2	-0.9	0.2
2	**5 + 5 ⇋ 11E/11Z + H_2O**	26.8	-0.2[b] / 2.5[c]	28.6	-0.3[b] / 2.5[c]	1.8	-0.1[b] / 0.0[c]
3	**11E/11Z + 4 + 4 ⇋ 16 + 2 + 2**	21.4[b] / 21.2[c]	-14.2[b] / -16.9[c]	22.4[b] / 20.7[c]	-14.4[b] / -17.2[c]	1.0[b] / -0.5[c]	-0.2[b] / 0.3[c]
4	**4 ⇋ 2 + $H_{2(sol)}$**	20.6	-1.3	22.9	-1.4	2.3	-0.1

[a]*All the energies are reported in kcal/mol.*
[b]*E conformer.*
[c]*Z conformer.*

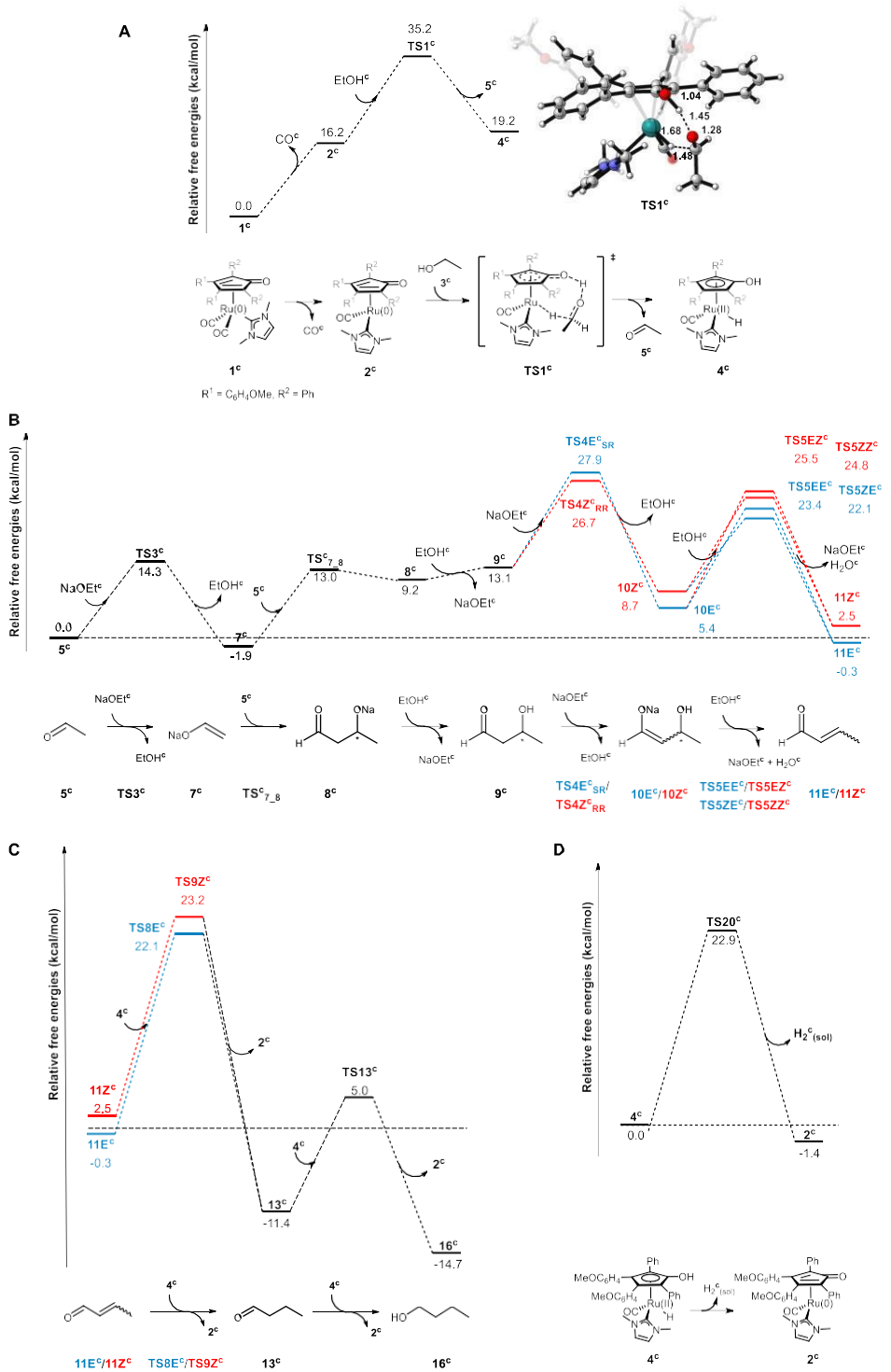

***Scheme S5**. Calculated free energy profiles for (**A**) the activation of the pre-catalyst (**1c**) and the dehydrogenation of ethanol (**3c**) to acetaldehyde (**5c**), and (top right) the optimized geometry of **TS1c**; (**B**) the base-catalyzed aldol condensation of two equivalents of **5c** to (E/Z)-crotonaldehyde (**11Ec/11Zc**) and (**C**) their double hydrogenation to 1-butanol (**16**); (**D**) the molecular hydrogen evolution process. DFT computations were carried out at the B3LYP-D3/6-311+G(2d,2p)/LANL2DZ/PCM(ethanol)//B3LYP-D3/6-31G(d,p)/LANL2DZ/PCM(ethanol) level of theory. The superscript "c" indicates stationary points with optimized geometries computed at the B3LYP-D3/6-31G(d,p)/LANL2DZ/PCM(ethanol) level.*

S6. Details of kinetic simulations and additional results

S6.1 Homologation of ethanol to 1-hexanol

The kinetic network used in the simulations is summarized in Table S5 and consists of all the elementary steps reported in **Scheme 3** (main text) and **Scheme S4** and the two additional equilibria mentioned in the main text, i.e. the solution-gas equilibrium of molecular hydrogen and the acid/base equilibrium of sodium ethoxide. The rate constants *k* are calculated according to the Eyring equation (Equation 1) using the free energy barriers computed for the corresponding elementary step:

$$k = \frac{k_B T}{h} e^{\frac{-\Delta G^{\ddagger}}{RT}} \qquad \text{(Equation 1)}$$

where k_b is the Boltzmann constant, *T* is the temperature (i.e. 150 °C), *h* is the Planck constant, $\Delta G^{\ddagger}$ is the free energy barrier, and *R* is the universal constant of gasses. In the case of barrier-less processes, the rate constant is approximated by the pre-exponential coefficient of Equation 1 at 150 °C.

Table S5. *Elementary steps considered in the kinetic model. For each step, the free energy barrier for the forward ($\Delta G^{\ddagger}_{forward}$) and backward ($\Delta G^{\ddagger}_{backward}$) processes and the corresponding rates constants ($k_{forward}$ and $k_{backward}$, respectively) are listed.*

entry	Elementary step	TS	$\Delta G^{\ddagger}_{forward}$ [a]	$\Delta G^{\ddagger}_{backward}$ [a]	$k_{forward}$ [b]	$k_{backward}$ [b]
1	**1 ⇋ 2 + CO**	-	16.23	0	3.65E+04	8.81E+12
2	**2 + 3 ⇋ 4 + 5**	**TS1**	19.83	17.08	5.05E+02	1.33E+04
3	**5 + 6 ⇋ 3 + 7**	**TS3**	14.38	12.99	3.29E+05	1.72E+06
4	**5 + 7 ⇋ 8**	-	8.83	0	2.42E+08	8.81E+12
5	**3 + 8 ⇋ 6 + 9**	-	3.04	0	2.37E+11	8.81E+12
6	**6 + 9 ⇋ 3 + 10E**	**TS4E$_{SR}$**	13.45	16.30	9.96E+05	3.36E+04
7	**6 + 9 ⇋ 3 + 10Z**	**TS4Z$_{RR}$**	13.54	14.38	8.95E+05	3.29E+05
8	**3 + 10E ⇋ 6 + H2O + 11E**	**TS5EE**	14.36	25.00	3.37E+05	1.08E+00
9	**3 + 10E ⇋ 6 + H2O + 11Z**	**TS5EZ**	16.81	24.74	1.83E+04	1.47E+00
10	**3 + 10Z ⇋ 6 + H2O + 11E**	**TS5ZE**	9.64	22.31	9.25E+07	2.64E+01
11	**3 + 10Z ⇋ 6 + H2O + 11Z**	**TS5ZZ**	12.58	22.53	2.80E+06	2.03E+01
12	**4 + 11E ⇋ 2 + 13**	**TS8E**	21.45	32.51	7.35E+01	1.42E-04
13	**4 + 11Z ⇋ 2 + 13**	**TS9Z**	21.23	35.00	9.55E+01	7.37E-06
14	**4 + 13 ⇋ 2 + 16**	**TS13**	16.38	19.47	3.05E+04	7.74E+02
15	**7 + 13 ⇋ 17**	**TS17**	11.92	2.84	6.14E+06	3.01E+11
16	**3 + 17 ⇋ 6 + 18**	**N/A**	2.98	0	2.55E+11	8.81E+12
17	**6 + 18 ⇋ 3 + 19E**	**TS18E$_{SR}$**	13.13	20.20	1.46E+06	3.25E+02
18	**6 + 18 ⇋ 3 + 19Z**	**TS18Z$_{RR}$**	12.96	15.08	1.78E+06	1.43E+05
19	**3 + 19E ⇋ 6 + H2O + 20E**	**TS19EE**	18.90	25.93	1.52E+03	3.57E-01
20	**3 + 19E ⇋ 6 + H2O + 20Z**	**TS19EZ**	20.60	25.01	2.02E+02	1.07E+00
21	**3 + 19Z ⇋ 6 + H2O + 20E**	**TS19ZE**	10.84	22.82	2.22E+07	1.44E+01
22	**3 + 19Z ⇋ 6 + H2O + 20Z**	**TS19ZZ**	13.88	23.25	5.97E+05	8.64E+00
23	**4 + 20E ⇋ 2 + 22**	**TS24E**	21.25	32.59	9.32E+01	1.30E-04
24	**4 + 20Z ⇋ 2 + 22**	**TS23Z**	20.19	34.14	3.29E+02	2.05E-05
25	**4 + 22 ⇋ 2 + 25**	**TS30**	15.97	19.00	4.97E+04	1.35E+03

Table S5 *continued.*

entry	Elementary step	TS	$\Delta G^{\ddagger}_{forward}$ [a]	$\Delta G^{\ddagger}_{backward}$ [a]	$k_{forward}$ [b]	$k_{backward}$ [b]
26	**4 ⇋ 2 + $H_{2(sol)}$**	**TS20**	20.57	21.83	2.09E+02	4.68E+01
27[c]	**$H_{2(sol)}$ ⇋ $H_{2(gas)}$**	-	-	-	1.00E-01	1.00E-02
28[c]	**6 + H_2O ⇋ 3 + NaOH**	-	-	-	4.00E+04	1.00E-01

[a] *All the energies are reported in kcal/mol.*
[b] *The rate constants are given in $s^{-1}\cdot mol^{n}\cdot L^{-n}$, where n is (total order of the reaction-1).*
[c] *The rate constants of these steps were estimated as discussed in the description of the kinetic model.*

Since the reaction matrix composition is a time-evolving basic alcoholic solution diluted by the water formed during the aldol condensation and kept at 150 °C, it was not possible to find accurate reference data for the equilibrium constants for the solution-gas equilibrium of molecular hydrogen and the acid/base equilibrium of sodium ethoxide. Here, the values of equilibrium constants for these steps were approximated (entries 27 and 28, Table S5) as discussed below.

For the solution-gas equilibrium of molecular hydrogen we assumed that at 150 °C under stirring, most of the molecular hydrogen is in the gas-phase. Therefore, the equilibrium constant in the present kinetic model was set to K_{eq} = 10, which corresponds to a 1:10 solution:gas ratio. Using this value in the kinetics simulations reproduces the conversion of the ethanol and the yields of all products quite well, as reported in the main text. When the equilibrium constant is increased up to get a 1:100 solution:gas ratio, the yield of the molecular hydrogen is overestimated, as well as the conversion of the ethanol (**Figure S9**). On the other hand, when the equilibrium constant is lowered to K_{eq} = 1, the overall reaction is slowed down significantly (**Figure S9**).

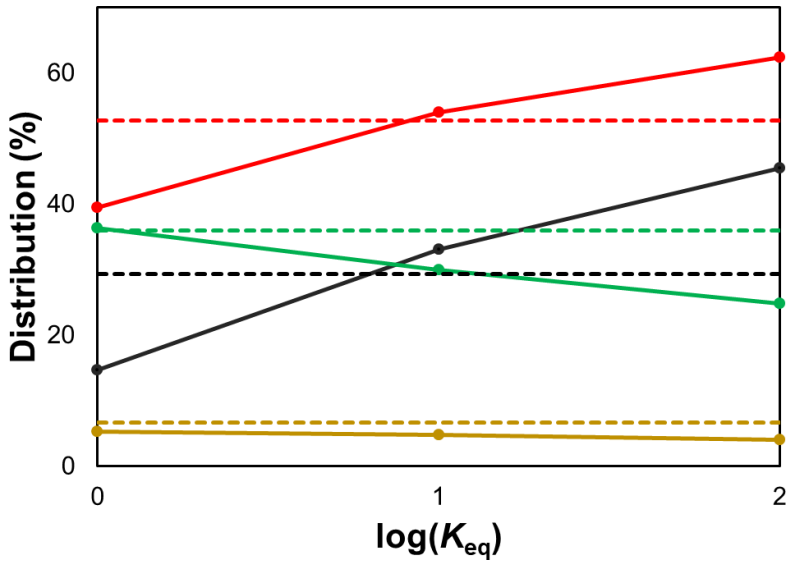

Figure S9. *Product distribution dependence on the value of the log(K_{eq}) governing the [$H_{2(sol)}$ ⇋ $H_{2(gas)}$] equilibrium with pK_b(NaOEt) = -5.6. The conversion of ethanol (red), the yield of 1-butanol (green), the yield of C_6 alcohols (orange) and the yield of molecular hydrogen (black) are reported. The solid lines are data from simulations, while the dashed lines are the corresponding experimental values.*

Next, to estimate the acid/base equilibrium constant of sodium ethoxide, the optimal pK_b of NaOEt was set to -5.6 since it is a very strong organic base. 10-fold variations of the equilibrium constant, i.e. 1-unit variation in the pK_b value, affect mainly the conversion of the ethanol. The lower the pK_b, the lower the conversion (**Figure S10**). This outcome is not surprising, since high basicity of NaOEt means that the concentration of the base is lowered, hampering the aldol condensation and, thus, the conversion of ethanol.

It is worth mentioning that the approximation of these equilibrium constants could partially compensate for the errors deriving from neglecting side processes in the simulations, like for instance the Cannizzaro and the Tishchenko reactions (**Scheme S1**). If included, these processes would consume a fraction of the aldehydes (i.e. **5** and **13**) and base, altering both the yields and the selectivities of the reaction. For example, when the solution-gas equilibrium involving the molecular hydrogen is added, the thermodynamics of the step governing the release of molecular hydrogen by **4** is modified. Such a variation decreases the concentration of **4** available to hydrogenate the products of the aldol condensation, lowering the yield of alcohols and the selectivity to them (**Figure S9**). Therefore, due to this equilibrium, there is a compensation for the lower yield of alcohols expected due to action of the Cannizzaro and Tishchenko side processes.

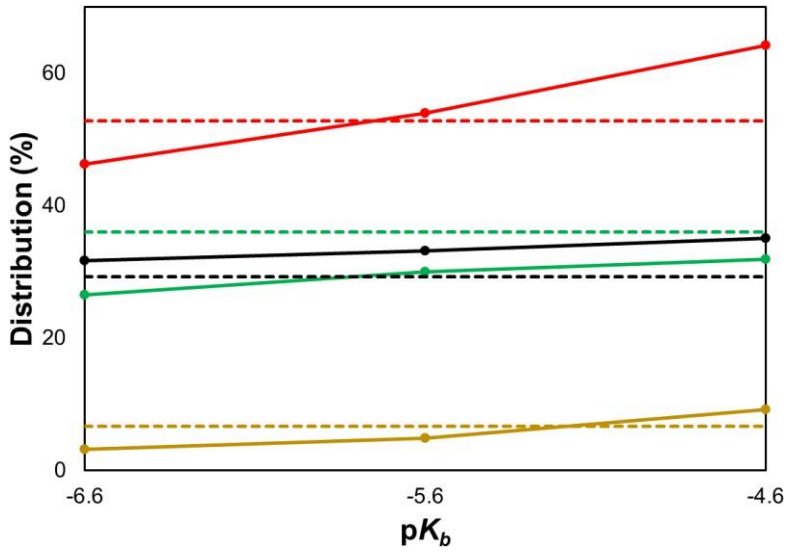

Figure S10. *Product distribution dependence on the value of the pK_b governing the [NaOEt + H_2O ⇋ EtOH + NaOH] equilibrium, with $K_{eq}(H_2)$ = 10. The conversion of ethanol (red), the yield of 1-butanol (green), the yield of C_6 alcohols (orange) and the yield of molecular hydrogen (black) are reported. The solid lines are data from simulations, while the dashed lines are the corresponding experimental values.*

S6.2 Including solvation and dispersions effects during geometry optimizations.

In Section S5, we showed that the choice of the geometry optimization method (with or without solvation and dispersions effect) does not have substantial effect on the characterization of the Guerbet reaction mechanism. Here, we report what is the effect on the kinetic network simulations. The kinetic network obtained including solvation and dispersions effects during geometry optimizations, i.e. at the B3LYP-D3/6-311+G(2d,2p)/LANL2DZ/PCM(ethanol)//B3LYP-D3/6-31G(d,p)/LANL2DZ/PCM level of theory, is reported in **Table S6**. This kinetic network consists of all the elementary steps reported in **Scheme S5** and the two additional equilibria mentioned in the main text, i.e. the solution-gas equilibrium of molecular hydrogen and the acid/base equilibrium of sodium ethoxide (entries 27 and 28 in **Table S5**).

Table S6. *Elementary steps considered in the kinetic model. For each step, the free energy barrier for the forward ($\Delta G^{\ddagger}_{forward}$) and backward ($\Delta G^{\ddagger}_{backward}$) processes and the corresponding rates constants ($k_{forward}$ and $k_{backward}$, respectively) are listed. The superscript "c" indicates stationary points with optimized geometries computed at the B3LYP-D3/6-31G(d,p)/LANL2DZ/PCM(ethanol) level.*

entry	Elementary step	TS	$\Delta G^{\ddagger}_{forward}$ [a]	$\Delta G^{\ddagger}_{backward}$ [a]	$k_{forward}$ [b]	$k_{backward}$ [b]
1	$\mathbf{1^c \leftrightharpoons 2^c + CO^c}$	N/A	16.16	0.00	3.97E+04	8.81E+12
2	$\mathbf{2^c + 3^c \leftrightharpoons 4^c + 5^c}$	$\mathbf{TS1^c}$	19.08	16.07	1.23E+03	4.42E+04
3	$\mathbf{5^c + 6^c \leftrightharpoons 3^c + 7^c}$	$\mathbf{TS3^c}$	14.34	16.28	3.46E+05	3.44E+04
4	$\mathbf{5^c + 7^c = 8^c}$	$\mathbf{TS^c_{7\_8}}$	14.98	3.81	1.61E+05	9.49E+10
5	$\mathbf{3^c + 8^c \leftrightharpoons 6^c + 9^c}$	N/A	3.87	0.00	8.84E+10	8.81E+12
6	$\mathbf{6^c + 9^c \leftrightharpoons 3^c + 10E^c}$	$\mathbf{TS4E^c_{SR}}$	14.83	22.50	1.93E+05	2.11E+01
7	$\mathbf{6^c + 9^c \leftrightharpoons 3^c + 10Z^c}$	$\mathbf{TS4Z^c_{RR}}$	13.55	17.93	8.84E+05	4.83E+03
8	$\mathbf{3^c + 10E^c \leftrightharpoons 6^c + H_2O^c + 11E^c}$	$\mathbf{TS5EE^c}$	17.94	23.64	4.78E+03	5.43E+00
9	$\mathbf{3^c + 10E^c \leftrightharpoons 6^c + H_2O^c + 11Z^c}$	$\mathbf{TS5EZ^c}$	20.08	23.06	3.75E+02	1.08E+01
10	$\mathbf{3^c + 10Z^c \leftrightharpoons 6^c + H_2O^c + 11E^c}$	$\mathbf{TS5ZE^c}$	13.36	22.36	1.11E+06	2.49E+01
11	$\mathbf{3^c + 10Z^c \leftrightharpoons 6^c + H_2O^c + 11Z^c}$	$\mathbf{TS5ZZ^c}$	16.09	22.38	4.31E+04	2.43E+01
12	$\mathbf{4^c + 11E^c \leftrightharpoons 2^c + 13^c}$	$\mathbf{TS8E^c}$	22.41	33.53	2.35E+01	4.23E-05
13	$\mathbf{4^c + 11Z^c \leftrightharpoons 2^c + 13^c}$	$\mathbf{TS9Z^c}$	20.73	34.57	1.73E+02	1.23E-05
14	$\mathbf{4^c + 13^c \leftrightharpoons 2^c + 16^c}$	$\mathbf{TS13^c}$	16.41	19.71	2.95E+04	5.82E+02
15	$\mathbf{4^c \leftrightharpoons 2^c + H_2{}^c}_{(sol)}$	$\mathbf{TS20^c}$	22.93	24.37	1.26E+01	2.28E+00
16 [d]	$\mathbf{H_2{}^c}_{(sol)} \leftrightharpoons \mathbf{H_2{}^c}_{(gas)}$	N/A	N/A	N/A	1.00E-01	1.00E-02
17 [d]	$\mathbf{6^c + H_2O^c \leftrightharpoons 3^c + NaOH^c}$	N/A	N/A	N/A	4.00E+04	1.00E-01

[a] *All the energies are reported in kcal/mol.*
[b] *The rate constants are given in $s^{-1}\cdot mol^{n}\cdot L^{-n}$, where n is (total order of the reaction-1).*
[d] *These steps correspond to entries 27 and 28 in **Table S5**.*

The complete kinetic network reported in the main text also includes the homologation of 1-butanol to 1-hexanol. While considering the latter, the size of the compounds involved in the reactions increases and the same for the computational time of the B3LYP-D3/6-311+G(2d,2p)/LANL2DZ/
PCM(ethanol)//B3LYP-D3/6-31G(d,p)/LANL2DZ/PCM(ethanol) calculations. However, one can reasonably assume that the energetics of the elementary steps to homologate of 1-butanol to 1-hexanol are the same of the homologation of ethanol to 1-butanol. In fact, we could validate this assumption by considering the simulations (reported in the main text) using gas-phase and

dispersion-free optimized geometries. **Figure S11** shows, indeed, comparable time-evolving ethanol conversion and distribution of products obtained using the complete network or the approximated one, i.e. assuming that the energetics of 1-butanol to 1-hexanol homologation parallel those of ethanol to 1-butanol.

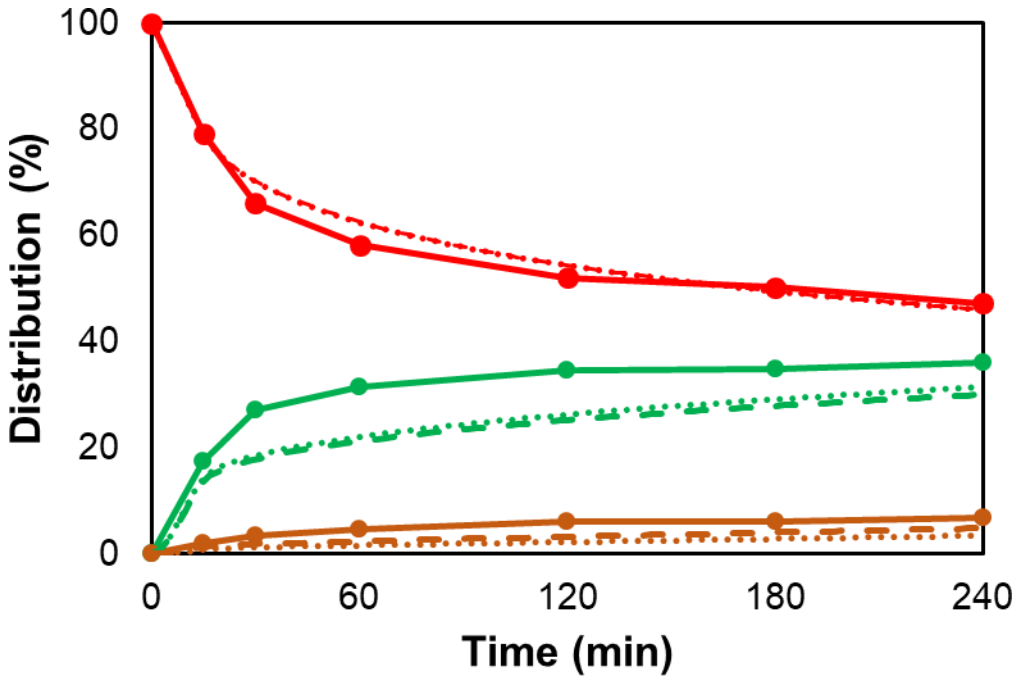

Figure S11. *Experimental (solid lines) and simulated time-evolving ethanol conversion and distribution of products using the model reported in the main text (dashed lines) or the approximated model assuming the energetics to homologate of 1-butanol to 1-hexanol the same as those of ethanol to 1-butanol (dotted lines). Residual ethanol (in red), yields of 1-butanol (in green) and 1-hexanol (in brown) are reported. Initial concentrations: [**1**]$_0$ = 0.03424 mol/L, [EtOH]$_0$ = 17.12 mol/L, and [NaOEt]$_0$ = 3.287 mol/L.*

This validated assumption can be applied to the kinetic model of the ethanol to 1-butanol homologation computed including solvation and dispersions effects during geometry optimizations, using the energetics of 1-butanol to 1-hexanol from the B3LYP-D3/6-311+G(2d,2p)/LANL2DZ/PCM(ethanol)//B3LYP-D3/6-31G(d,p)/LANL2DZ/PCM(ethanol) data reported in **Table S6**. As shown in **Figure S12**, this allows for a comparison between the time-evolving conversion and products distribution using different methods for the geometry optimizations. The comparison of the two simulations shows that including solvation and dispersions effects during geometry optimizations does not significantly affect the kinetic network simulations. The more accurate (and more computationally expensive) geometry optimization method returns final product distribution in better agreement with experimental data, with a yield in 1-butanol of 40% (*vs* 36% in experiments), a yield in total alcohols of 47% (*vs* 47% in experiments), and a yield of molecular hydrogen of 21% (*vs* 29% in experiments), reproducing a selectivity to total alcohols of 89%. Not surprisingly, the increase of some activation barriers discussed above, see **Tables S3** and **S4**, on the other hand, increases the end-of-reaction simulation time by ca. 5 times (**Figure S12A**), which is thus normalized in **Figure S12B**.

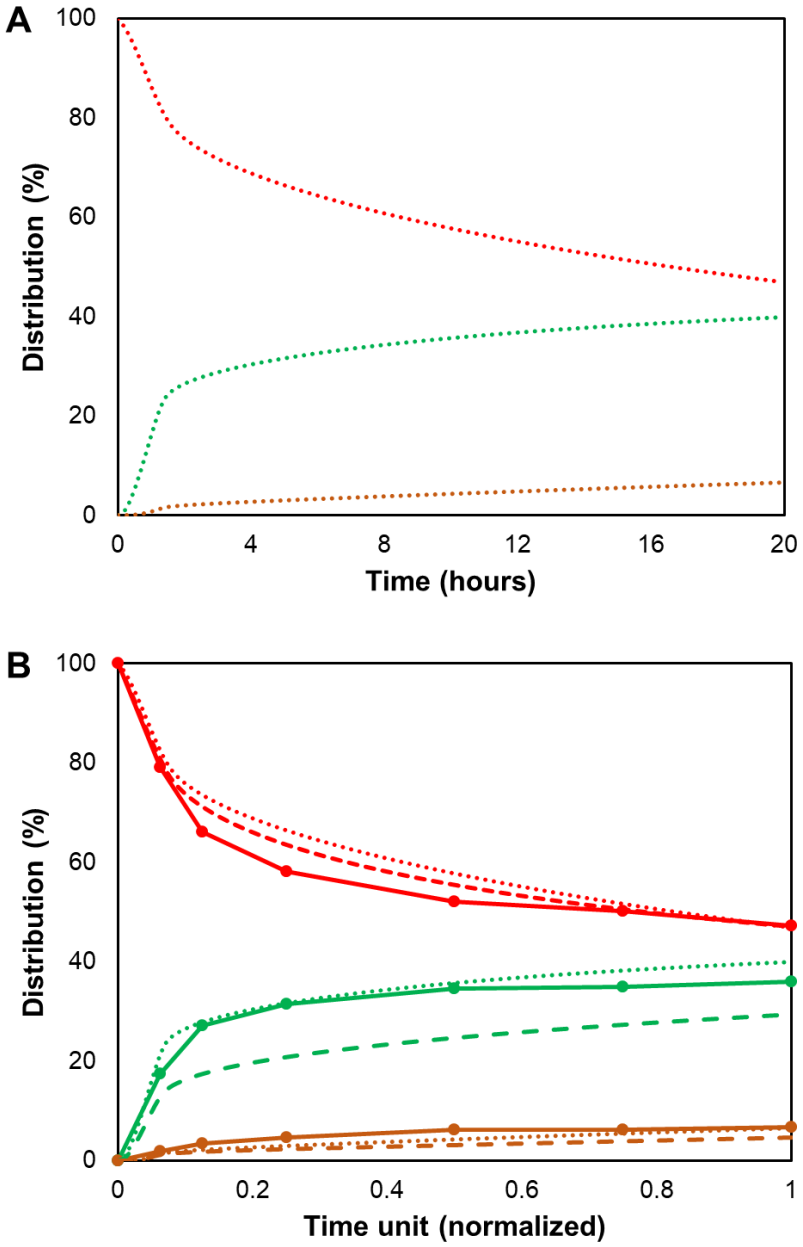

Figure S12. *(A) Simulated time-evolving ethanol conversion and distribution of products using B3LYP-D3/6-31G(d,p)/LANL2DZ/PCM(ethanol) as geometry optimization method. (B) Comparison between experimental (solid lines) and simulated time-evolving ethanol conversion and distribution of products using B3LYP-D3/6-31G(d,p)/LANL2DZ/PCM(ethanol) (dotted lines) or B3LYP/6-31G(d,p)/LANL2DZ (dashed lines) as geometry optimization method. Time is normalized. In both panels, product distribution is reported at iso-conversion with respect to the experimental value (i.e. 53%). Residual ethanol (in red), yields of 1-butanol (in green) and 1-hexanol (in brown) are reported. Initial concentrations:* $[1]_0$ *= 0.03424 mol/L,* $[EtOH]_0$ *= 17.12 mol/L, and* $[NaOEt]_0$ *= 3.287 mol/L.*

S7. Conversion, yields and carbon loss definitions

In the following, the formula used in the present work are reported:

- $\boldsymbol{Conversion}\ (\%) = \frac{[\boldsymbol{EtOH}]}{[\boldsymbol{EtOH}]_{\boldsymbol{0}}}\ \boldsymbol{100}$

- $\boldsymbol{Yield_{C_nOH}}\ (\%) = \frac{\boldsymbol{n}\ [\boldsymbol{C_nOH}]}{\boldsymbol{2}\ [\boldsymbol{EtOH}]_{\boldsymbol{0}}}\ \boldsymbol{100}$

- $\boldsymbol{Yield_{ROH}}\ (\%) = \sum_n \frac{\boldsymbol{n}\ [\boldsymbol{C_nOH}]}{\boldsymbol{2}\ [\boldsymbol{EtOH}]_{\boldsymbol{0}}}\ \boldsymbol{100}$

- $\boldsymbol{Yield_{H_2}}\ (\%) = \frac{[\boldsymbol{H_2}]}{[\boldsymbol{EtOH}]_{\boldsymbol{0}}}\ \boldsymbol{100}$

- $\boldsymbol{C_{loss}}\ (\%) = \boldsymbol{Conversion}\ (\%) - \boldsymbol{Yield_{ROH}}\ (\%)$

with $[\boldsymbol{EtOH}]_{\boldsymbol{0}}$ representing initial concentration of ethanol and *n* is the number of C atoms in higher alcohol, i.e. n>2.

S8. Absolute energies and energy corrections

In **Table S7** absolute energies and energy correction with imaginary frequencies of all the intermediates and transition states are reported.

Table S7*. Absolute energies and energy corrections (a.u.) along with imaginary frequencies of TSs.*

entry	Stationary point	B3LYP/ 6-31G(d,p)/ LANL2DZ optimization	Thermal correction to Gibbs free energy	B3LYP-D3/ 6-311+G(2d,2p)/ LANL2DZ (PCM, single-point)	Total energy	Imaginary frequency (cm-1)
1	**CO**	-113.306912	-0.02377	-113.352323	-113.376091	-
2	**H_2**	-1.178539	-0.00778	-1.180168	-1.187944	-
3	**H_2O**	-76.41816	-0.00557	-76.468663	-76.474231	-
4	**NHC**	-304.797265	0.078199	-304.907169	-304.82897	-
5	**1**	-2046.88839	0.476275	-2047.5942	-2047.11792	-
6	**2**	-1933.52445	0.468569	-1934.18453	-1933.71596	-
7	**3**	-155.043856	0.041496	-155.109704	-155.068208	-
8	**4**	-1934.72884	0.487292	-1935.38919	-1934.9019	-
9	**5**	-153.832733	0.017632	-153.89551	-153.877878	-
10	**6**	-316.746134	0.023257	-316.861427	-316.83817	-
11	**7**	-315.538597	0.003347	-315.648977	-315.64563	-
12	**8**	-469.408476	0.054339	-469.563774	-469.509435	-
13	**9**	-307.68184	0.070706	-307.805327	-307.734621	-
14	**10E**	-469.386918	0.053103	-469.562237	-469.509134	-
15	**10Z**	-469.405945	0.057654	-469.563567	-469.505913	-
16	**11E**	-231.238222	0.045398	-231.327298	-231.2819	-
17	**11Z**	-231.233877	0.045454	-231.323038	-231.277584	-
18	**12E**	-232.438713	0.066989	-232.532106	-232.465117	-
19	**12Z**	-232.436134	0.066647	-232.529796	-232.463149	-
20	**13**	-232.463909	0.066638	-232.552094	-232.485456	-
21	**14E**	-394.170984	0.05178	-394.305343	-394.253563	-
22	**14Z**	-394.164971	0.048715	-394.3067	-394.257985	-
23	**15E**	-232.448283	0.068328	-232.537287	-232.468959	-
24	**15Z**	-232.4477	0.067718	-232.53733	-232.469612	-
25	**16**	-233.674781	0.090294	-233.766595	-233.676301	-
26	**17**	-548.038726	0.103403	-548.220013	-548.11661	-
27	**18**	-386.312231	0.119995	-386.461899	-386.341904	-
28	**19E**	-548.012264	0.10022	-548.223344	-548.123124	-
29	**19Z**	-548.038449	0.106523	-548.221752	-548.115229	-
30	**20E**	-309.869719	0.094485	-309.984611	-309.890126	-
31	**20Z**	-309.86536	0.094492	-309.980455	-309.885963	-
32	**21E**	-311.070223	0.116148	-311.189468	-311.07332	-
33	**21Z**	-311.067573	0.115763	-311.187198	-311.071435	-
34	**22**	-311.095615	0.115715	-311.209844	-311.094129	-
35	**23E**	-472.802806	0.100689	-472.963067	-472.862378	-
36	**23Z**	-472.79712	0.098937	-472.964594	-472.865657	-
37	**24E**	-311.077013	0.116262	-311.194282	-311.07802	-
38	**24Z**	-311.077486	0.115936	-311.194875	-311.078939	-

Table S7 *continued.*

entry	Stationary point	B3LYP/ 6-31G(d,p)/ LANL2DZ optimization	Thermal correction to Gibbs free energy	B3LYP-D3/ 6-311+G(2d,2p)/ LANL2DZ (PCM, single-point)	Total energy	Imaginary frequency (cm-1)
39	**25**	-312.306405	0.139339	-312.424229	-312.28489	-
40	**26**	-1742.01556	0.359753	-1742.60504	-1742.24528	-
41	**27**	-1743.23101	0.380053	-1743.82109	-1743.44104	-
42	**TS1**	-2088.56327	0.538598	-2089.29116	-2088.75256	-467.7
43	**TS2**	-2088.56128	0.538694	-2089.29004	-2088.75135	-386.8
44	**TS3**	-470.609169	0.064244	-470.757382	-470.693138	-872.2
45	**TS4E$_{RR}$**	-624.450403	0.116366	-624.663662	-624.547296	-676.8
46	**TS4E$_{SR}$**	-624.453693	0.11641	-624.667769	-624.551359	-747.5
47	**TS4Z$_{RR}$**	-624.453233	0.116917	-624.668125	-624.551208	-643.7
48	**TS4Z$_{SR}$**	-624.468041	0.11949	-624.668608	-624.549118	-452.1
49	**TS5EE**	-624.453044	0.112771	-624.66723	-624.554459	-485.6
50	**TS5EZ**	-624.450024	0.113058	-624.663615	-624.550557	-447.9
51	**TS5ZE**	-624.470501	0.115608	-624.674359	-624.558751	-131.4
52	**TS5ZZ**	-624.464556	0.115353	-624.669428	-624.554075	-120.1
53	**TS6E**	-2165.96466	0.564419	-2166.71816	-2166.15374	-652.7
54	**TS6Z**	-2165.9614	0.564294	-2166.71473	-2166.15043	-647
55	**TS7E**	-2165.96125	0.563505	-2166.71714	-2166.15364	-641.3
56	**TS7Z**	-2165.95801	0.563909	-2166.71503	-2166.15112	-626.1
57	**TS8E**	-2165.94598	0.565522	-2166.71513	-2166.14961	-182.9
58	**TS8Z**	-2165.93875	0.566509	-2166.70836	-2166.14186	-263
59	**TS9E**	-2165.9472	0.565986	-2166.71409	-2166.1481	-305.2
60	**TS9Z**	-2165.94323	0.566	-2166.71164	-2166.14564	-212.2
61	**TS10E**	-549.239688	0.113067	-549.41407	-549.301003	-912.3
62	**TS10Z**	-549.239316	0.114029	-549.414499	-549.30047	-863.1
63	**TS11E**	-2167.1389	0.58362	-2167.89817	-2167.31455	-1186.9
64	**TS11Z**	-2167.13547	0.583836	-2167.89647	-2167.31263	-1105
65	**TS12E**	-2167.13156	0.584549	-2167.89562	-2167.31107	-1206.8
66	**TS12Z**	-2167.13494	0.583377	-2167.8983	-2167.31492	-1224.6
67	**TS13**	-2167.19415	0.588913	-2167.95016	-2167.36124	-530.9
68	**TS14**	-2167.19157	0.58881	-2167.94817	-2167.35936	-457
69	**TS15E**	-2167.13927	0.586219	-2167.90227	-2167.31605	-1160
70	**TS15Z**	-2167.13588	0.585701	-2167.89921	-2167.31351	-1131.1
71	**TS16E**	-2167.13821	0.586167	-2167.90198	-2167.31581	-1043.5
72	**TS16Z**	-2167.13805	0.586468	-2167.90196	-2167.3155	-1209.1
73	**TS17**	-548.029904	0.098743	-548.210829	-548.112086	-80.1
74	**TS18E$_{RR}$**	-703.081692	0.165571	-703.320628	-703.155057	-728.5
75	**TS18E$_{SR}$**	-703.085523	0.165734	-703.324878	-703.159144	-750.6
76	**TS18Z$_{RR}$**	-703.085047	0.166161	-703.325574	-703.159413	-645.4
77	**TS18Z$_{SR}$**	-703.099561	0.168574	-703.325933	-703.157359	-483.5
78	**TS19EE**	-703.085504	0.162912	-703.324118	-703.161206	-478.4
79	**TS19EZ**	-703.081976	0.162574	-703.321081	-703.158507	-463
80	**TS19ZE**	-703.104757	0.165769	-703.331925	-703.166156	-121.8

Table S7 *continued.*

entry	Stationary point	B3LYP/ 6-31G(d,p)/ LANL2DZ optimization	Thermal correction to Gibbs free energy	B3LYP-D3/ 6-311+G(2d,2p)/ LANL2DZ (PCM, single-point)	Total energy	Imaginary frequency (cm-1)
81	**TS19ZZ**	-703.095422	0.165573	-703.326889	-703.161316	-96.6
82	**TS20**	-2089.75785	0.551025	-2090.48835	-2089.93732	-876.3
83	**TS21**	-2011.13795	0.505391	-2011.84282	-2011.33742	-875.2
84	**TS22**	-1934.66157	0.484035	-1935.32804	-1934.84401	-1753.7
85	**TS23E**	-2244.57568	0.615506	-2245.37178	-2244.75627	-410.8
86	**TS23Z**	-2244.57287	0.615216	-2245.3709	-2244.75569	-276.9
87	**TS24E**	-2244.57448	0.615321	-2245.37348	-2244.75816	-427.5
88	**TS24Z**	-2244.56705	0.614844	-2245.36583	-2244.75099	-272.8
89	**TS25E**	-2244.59621	0.613456	-2245.37575	-2244.76229	-650
90	**TS25Z**	-2244.59291	0.613046	-2245.37246	-2244.75942	-639.2
91	**TS26E**	-2244.58986	0.614404	-2245.37276	-2244.75836	-416.3
92	**TS26Z**	-2244.58737	0.613122	-2245.37165	-2244.75852	-401.7
93	**TS27E**	-627.871476	0.16226	-628.071984	-627.909724	-910.6
94	**TS27Z**	-627.871253	0.162976	-628.072427	-627.909451	-857.4
95	**TS28E**	-2245.77068	0.632946	-2246.55658	-2245.92363	-1201.6
96	**TS28Z**	-2245.76715	0.633464	-2246.55492	-2245.92146	-1104.3
97	**TS29E**	-2245.76315	0.633114	-2246.55485	-2245.92173	-1226.5
98	**TS29Z**	-2245.76694	0.632689	-2246.55748	-2245.92479	-1232.1
99	**TS30**	-2245.8258	0.63786	-2246.60843	-2245.97057	-529.2
100	**TS31**	-2245.82326	0.637429	-2246.60643	-2245.969	-455.5
101	**TS32E**	-2245.76763	0.634844	-2246.55945	-2245.9246	-1209
102	**TS32Z**	-2245.76536	0.634935	-2246.55855	-2245.92361	-1196.6
103	**TS33E**	-2245.76714	0.634977	-2246.56109	-2245.92611	-1117.6
104	**TS33Z**	-2245.76878	0.636291	-2246.56046	-2245.92417	-1214
105	**TS34**	-1897.05793	0.42539	-1897.71245	-1897.28706	-861.3
106	**1**[c]	-2047.025244	0.479459	-2047.595505	-2047.116046	-
107	**CO**[c]	-113.307586	-0.023777	-113.352328	-113.376105	-
108	**2**[c]	-1933.656687	0.473083	-1934.187272	-1933.714189	-
109	**3**[c]	-155.051697	0.041430	-155.109769	-155.068339	-
110	**4**[c]	-1934.860324	0.491074	-1935.390916	-1934.899842	-
111	**5**[c]	-153.839650	0.017676	-153.895562	-153.877886	-
112	**6**[c]	-316.796464	0.022164	-316.864402	-316.842238	-
113	**7**[c]	-315.584554	0.000140	-315.655007	-315.654867	-
114	**8**[c]	-469.452664	0.052506	-469.567456	-469.514950	-
115	**9**[c]	-307.698216	0.070612	-307.805496	-307.734884	-
116	**10E**[c]	-469.446319	0.049672	-469.570676	-469.521004	-
117	**10Z**[c]	-469.454586	0.053730	-469.569483	-469.515753	-
118	**11E**[c]	-231.249108	0.045442	-231.327401	-231.281959	-
119	**11Z**[c]	-231.245069	0.045505	-231.323134	-231.277629	-
120	**13**[c]	-232.475827	0.066850	-232.552182	-232.485332	-
121	**16**[c]	-233.687707	0.090413	-233.766658	-233.676245	-
122	**H_2O**[c]	-76.424827	-0.005608	-76.468630	-76.474238	-

Table S7 *continued.*

entry	Stationary point	B3LYP/ 6-31G(d,p)/ LANL2DZ optimization	Thermal correction to Gibbs free energy	B3LYP-D3/ 6-311+G(2d,2p)/ LANL2DZ (PCM, single-point)	Total energy	Imaginary frequency (cm-1)
123	H_2[c]	-1.178668	-0.007780	-1.180168	-1.187948	-
124	**TS1**[c]	-2088.713400	0.541233	-2089.293357	-2088.752124	-338.5
125	**TS3**[c]	-470.648934	0.064408	-470.761675	-470.697267	-852.9
126	$TS^{c}_{7\_8}$	-469.442704	0.049578	-469.558460	-469.508882	-152.7
127	$TS4E^{c}_{SR}$	-624.505146	0.116419	-624.669911	-624.553492	-617.0
128	$TS4Z^{c}_{RR}$	-624.506856	0.116624	-624.672146	-624.555522	-581.4
129	**TS5EE**[c]	-624.503063	0.114846	-624.675605	-624.560759	-614.2
130	**TS5EZ**[c]	-624.498486	0.113423	-624.670774	-624.557351	-694.1
131	**TS5ZE**[c]	-624.512323	0.117905	-624.680706	-624.562801	-166.4
132	**TS5ZZ**[c]	-624.506261	0.116628	-624.675076	-624.558448	-163.4
133	**TS8E**[c]	-2166.111188	0.570894	-2166.716987	-2166.146093	-342.4
134	**TS9Z**[c]	-2166.107736	0.569158	-2166.713591	-2166.144433	-436.8
135	**TS13**[c]	-2167.353466	0.593847	-2167.952864	-2167.359017	-465.6
136	**TS20**[c]	-2089.909633	0.558545	-2090.490179	-2089.931634	-844.0

S9. References

1. Cesari, C., Conti, S., Zacchini, S., Zanotti, V., Cassani, M.C., and Mazzoni, R. (2014). Sterically driven synthesis of ruthenium and ruthenium–silver N-heterocyclic carbene complexes. Dalt. Trans. *43*, 17240–17243. 10.1039/C4DT02747G.
2. Bradley, D.C., Mehrotra, R.C., Rothwell, I.P., and Singh, A. (2001). 2 - Homometallic Alkoxides. In Alkoxo and Aryloxo Derivatives of Metals, D. C. Bradley, R. C. Mehrotra, I. P. Rothwell, and A. Singh, eds. (Academic Press), pp. 3–181. 10.1016/B978-012124140-7/50002-5.
3. Riddick, J.A., Bunger, W.B., and Sakano, T.K. (1985). Techniques of chemistry fourth edition, Volume II. Organic Solvents at John Wiley, New York, NY.
4. Messori, A., Gagliardi, A., Cesari, C., Calcagno, F., Tabanelli, T., Cavani, F., and Mazzoni, R. (2023). Advances in the homogeneous catalyzed alcohols homologation: the mild side of the Guerbet reaction. A mini-review. Catal. Today. 10.1016/j.cattod.2023.01.010.
5. Becke, A.D. (1993). Density-functional thermochemistry. III. The role of exact exchange. J. Chem. Phys. *98*, 5648–5652. 10.1063/1.464913.
6. Becke, A.D. (1992). Density-functional thermochemistry. II. The effect of the Perdew–Wang generalized-gradient correlation correction. J. Chem. Phys. *97*, 9173–9177. 10.1063/1.463343.
7. Becke, A.D. (1992). Density-functional thermochemistry. I. The effect of the exchange-only gradient correction. J. Chem. Phys. *96*, 2155–2160. 10.1063/1.462066.
8. Becke, A.D. (1988). Density-functional exchange-energy approximation with correct asymptotic behavior. Phys. Rev. A *38*, 3098–3100. 10.1103/PhysRevA.38.3098.
9. Lee, C., Yang, W., and Parr, R.G. (1988). Development of the Colle-Salvetti correlation-energy formula into a functional of the electron density. Phys. Rev. B *37*, 785–789.

10.1103/PhysRevB.37.785.
10. Frisch, M.J., Trucks, G.W., Schlegel, H.B., Scuseria, G.E., Robb, M.A., Cheeseman, J.R., Scalmani, G., Barone, V., Petersson, G.A., Nakatsuji, H., et al. (2016). Gaussian16 Revision A.03.
11. Francl, M.M., Pietro, W.J., Hehre, W.J., Binkley, J.S., Gordon, M.S., DeFrees, D.J., and Pople, J.A. (1982). Self-consistent molecular orbital methods. XXIII. A polarization-type basis set for second-row elements. J. Chem. Phys. *77*, 3654–3665. 10.1063/1.444267.
12. Hay, P.J., and Wadt, W.R. (1985). *Ab initio* effective core potentials for molecular calculations. Potentials for K to Au including the outermost core orbitals. J. Chem. Phys. *82*, 299–310. 10.1063/1.448975.
13. Scalmani, G., and Frisch, M.J. (2010). Continuous surface charge polarizable continuum models of solvation. I. General formalism. J. Chem. Phys. *132*, 114110. 10.1063/1.3359469.
14. Clark, T., Chandrasekhar, J., Spitznagel, G.W., and Schleyer, P.V.R. (1983). Efficient diffuse function-augmented basis sets for anion calculations. III. The 3-21+G basis set for first-row elements, Li–F. J. Comput. Chem. *4*, 294–301. 10.1002/jcc.540040303.
15. Frisch, M.J., Pople, J.A., and Binkley, J.S. (1984). Self-consistent molecular orbital methods 25. Supplementary functions for Gaussian basis sets. J. Chem. Phys. *80*, 3265–3269. 10.1063/1.447079.
16. McLean, A.D., and Chandler, G.S. (1980). Contracted Gaussian basis sets for molecular calculations. I. Second row atoms, Z=11–18. J. Chem. Phys. *72*, 5639–5648. 10.1063/1.438980.
17. Krishnan, R., Binkley, J.S., Seeger, R., and Pople, J.A. (1980). Self-consistent molecular orbital methods. XX. A basis set for correlated wave functions. J. Chem. Phys. *72*, 650–654. 10.1063/1.438955.
18. Grimme, S., Antony, J., Ehrlich, S., and Krieg, H. (2010). A consistent and accurate *ab initio* parametrization of density functional dispersion correction (DFT-D) for the 94 elements H-Pu. J. Chem. Phys. *132*, 154104. 10.1063/1.3382344.
19. Petzold, L. (1983). Automatic Selection of Methods for Solving Stiff and Nonstiff Systems of Ordinary Differential Equations. SIAM J. Sci. Stat. Comput. *4*, 136–148. 10.1137/0904010.
20. Hoops, S., Sahle, S., Gauges, R., Lee, C., Pahle, J., Simus, N., Singhal, M., Xu, L., Mendes, P., and Kummer, U. (2006). COPASI--a COmplex PAthway SImulator. Bioinformatics *22*, 3067–3074. 10.1093/bioinformatics/btl485.